Anomalous top couplings at hadron colliders revisited

Fabian Bach[*] and Thorsten Ohl[†]

Institut für Theoretische Physik und Astrophysik, Universität Würzburg, Hubland Nord,
97074 Würzburg, Germany
(Received 25 September 2012; published 20 December 2012)

In an effective operator approach, the full set of leading contributions to anomalous top couplings comprises various new trilinear as well as higher interaction vertices, some of which are related to one another by gauge symmetry or equations of motion. In order to study trilinear top couplings to Standard Model gauge bosons such as $tt\gamma$, ttZ, tbW and ttg, the operator set can be restricted accordingly. However, the complete basis cannot be mapped onto an on-shell parametrization of the trilinear vertices alone. Four-fermion contact terms $qqtt$ and $udtb$ must be included if the relation to the operator basis is to be retained. In this paper, we point out how these interactions contribute to the single top search channels for anomalous trilinear tbW couplings at the LHC and Tevatron, thus affecting the corresponding bounds. All results are based on full leading-order partonic matrix elements, thus automatically accounting for off-shell and interference effects as well as irreducible backgrounds. A discussion of the quantitative effects of going from on-shell tops to full matrix elements including acceptance cuts is also provided.

I. INTRODUCTION

The Standard Model (SM) of particle physics has stood its ground during the past decades with great success, consistently explaining and predicting a great variety of high-energy experiments with unchallenged precision. One of the major cornerstones was the discovery of the top quark at the Tevatron in 1995 [1,2], confirming the postulated three-family doublet structure of the SM. While the Tevatron experiments have continued to collect data and improve their measurements of top properties, most importantly its mass [3–6], most attention is now directed to the LHC up and running at $\sqrt{s} = 8$ TeV, and the results of its multipurpose experiments ATLAS and CMS improving on top statistics by the day. By now, top pair production has been measured in different channels with remarkable accuracy [7–12]. Single top production has already been established for $bg \rightarrow tW$ associated production despite its small cross section [13,14] and even been definitely observed in the dominant t channel $bq \rightarrow tq'$ [15–17]. The ever-growing abundance of top events at the LHC is beginning to allow the determination of more involved observables such as asymmetries, invariant pair mass distribution and top couplings to the other SM particles with high precision (cf. e.g., Refs. [18,19] for an overview).

On the theoretical side, the top quark takes an outstanding place among the spectrum of SM particles as a possible window to new non-SM physics because of its uniquely large mass of the order of the electroweak symmetry breaking scale $m_t \sim \upsilon \sim \mathcal{O}(100 \text{ GeV})$, with

its role within the dynamics of electroweak symmetry breaking still unresolved. Corresponding new physics effects in the top sector may manifest themselves in the deviation of top properties from their SM values, where the main attention in this paper is directed towards the trilinear couplings to SM gauge bosons, especially the charged-current (CC) interaction tbW. Therefore, even before any experimental analysis, a theoretically robust parametrization of these anomalous couplings has to be found, at the same time reducing the parameter space to an experimentally manageable minimum while staying fully general within the basis of effective operators generating these couplings at Lagrangian level. Indeed, starting from the complete set of effective dimension six operators as written down by Buchmüller and Wyler already in 1985 [20], substantial effort has been put into this task in the past decades by various authors [21–31]. The crucial ingredient of most of these analyses is to employ the theorem [32–36] that the field equations of motion (EOM) can safely be used at the Lagrangian level at a fixed order in the effective operator expansion in order to rewrite operators and identify redundant structures.

As a result of this procedure, it is often argued that these redundancies allow for a reduction of independent couplings to be incorporated in a phenomenological analysis of anomalous top couplings. However, as has been pointed out e.g., in Refs. [27,28] and will also be reviewed again in more detail later on, the application of the EOM necessarily generates four-fermion contact interactions, which are nevertheless often dropped from the analyses for the sake of simplicity. We note that the latter procedure does not correspond to a *rewriting* but rather to a *redefinition* of the originally chosen operator

_____
[*]fabian.bach@physik.uni-wuerzburg.de
[†]ohl@physik.uni-wuerzburg.de

basis, thus also departing from the full generality of the original basis with respect to the richness of structures in the trilinear couplings. Still, the operator equalities derived by various authors [27,28,37] and systematically presented in Ref. [28] are very useful to simplify an implementation of the most general set of trilinear top couplings into a Monte Carlo (MC) generator in a gauge-invariant way, so in our approach, rather than dropping part of the physics, we make use of these equalities to implement *all* the trilinear top couplings to SM gauge bosons in the language of on-shell couplings including the required quartic contact terms into the parton-level MC event generator WHIZARD [38], also addressing the interplay of anomalous top and bottom couplings—the latter already heavily bounded by LEP data—and the repercussions on the top couplings. Finally, we present phenomenological consequences obtained with our implementation for the parameter space of the anomalous couplings in the CC sector.

This paper is organized as follows: in Sec. II we review the procedure described above of defining a complete operator basis to generate anomalous top couplings to SM gauge bosons and applying the EOM to rewrite some of these operators, thus arriving at the most suitable form for a MC implementation. In Sec. III we discuss the LHC phenomenology with a focus on single top production, including a comparison of on-shell and full matrix element approaches to retrieve the cross sections at detector level as functions of the anomalous *tbW* couplings as well as a presentation of the physical effects and consequences of the newly added coupling structures. A discussion and summary of the main statements and results can be found in Sec. IV.

II. THEORETICAL SETUP

In order to be self-contained in this paper, we start this section by reviewing in some detail the main steps of the procedure presented in Ref. [28] to simplify the most general set of operators generating the trilinear anomalous top couplings to SM gauge bosons *ttγ*, *ttZ*, *tbW* and *ttg*. However, although we emphasize that all of these couplings are implemented in WHIZARD in a gauge-invariant way, including all quartic terms generated by the operator rewriting, we will restrict ourselves here to the discussion of the CC sector, i.e., only those operators generating anomalous contributions to the *tbW* interaction, for two simple reasons:

(1) the complexity of the parameter space in the CC sector is increased in a minimal way compared to previous studies [37,39–41], because it turns out that only one additional operator (and hence coupling) has to be considered;

(2) at hadron colliders, the experimental access to the new effects is most straightforward, combining

studies of CC single top production and of top decay products.[1]

In the following two subsections we develop the basic ingredients of the effective operator analysis, recapitulate the operator rewriting procedure and finally present our extended parameter space for the anomalous *tbW* couplings.

A. Effective operator approach and operator basis

There are basically two ways to tackle new physics beyond the SM in a systematic and consistent manner: Either the model building (top-down) approach, i.e., starting from a postulated Lagrangian—which incorporates a sensible UV completion—and deriving from it physical effects to which present or planned experiments might be sensitive, or the effective (bottom-up) approach, i.e., starting from the established SM symmetries and *a priori* considering *all* possible new physics effects compatible with these symmetries at the Lagrangian level, postponing the question which larger theory might generate the relevant parameters at a higher energy scale Λ.

Since we follow the second approach, it shall be clarified a little further. The idea is to confront new physics completely unbiased, that is without any assumptions about the dynamical degrees of freedom generating it, and to study the effects that are manifest at a testable energy scale (considerably smaller than the resonant scale Λ) where the degrees of freedom are the well-known SM particles. This corresponds to integrating out the heavy modes, thus generating effective operators $O_i^{(d)}$ of mass dimension $d > 4$ which are normalized by appropriate powers of Λ. In the model-independent approach, the effective Lagrangian can be written as an expansion in $1/\Lambda$ [20,47,48],

$$\mathcal{L}_{\text{eff}} = \mathcal{L}_{\text{SM}} + \sum_{d>4,i} \frac{C_i^{(d)}}{\Lambda^{d-4}} O_i^{(d)} + \text{H.c.}, \qquad (1)$$

---

[1]The anomalous NC sector, while of course related to the CC sector by gauge symmetry (cf. the end of Sec. II B), is much harder to access experimentally, because one would have to identify the final state *ttZ*, which is an even more complex analysis than the already challenging *ttγ* study due to the further reduced cross section and the necessity to reconstruct the decaying *Z*. In the QCD sector, anomalous *ttg* (and *ttgg*) chromomagnetic dipole couplings have been studied by Refs. [42–44]. The vectorlike *ttqq* operators which are related to the *ttg* sector by the EOM contribute only in the $q\bar{q} \rightarrow t\bar{t}$ amplitudes and are therefore suppressed by the parton distribution functions (pdfs) with respect to the dominant gluon fusion channel. Non-negligible effects of quartic *ttqq* couplings have been widely discussed in the literature as possible explanations of the $t\bar{t}$ forward-backward asymmetry observed at the Tevatron, cf. e.g., Refs. [45,46]. However, for this purpose axial *ttqq* couplings are required as well, which are not related to a vectorlike anomalous *ttg* sector by the EOM.

with dimensionless operator coefficients $C_i^{(d)}$, comprising *all* possible effective operators built from SM fields and derivatives only, and compatible with all local and global SM symmetries. A complete set of these operators for $d = 5, 6$ can be found in Ref. [20].

The only possible $d = 5$ operator in this setup is a neutrino mass term [20], so the leading contributions to anomalous trilinear top couplings must be $d = 6$. The complete operator list at this order can be found in Refs. [28–30], of which we now quote the ones relevant to trilinear tbW interactions (also adopting the nomenclature of Ref. [28]),

$$O_{\phi q}^{(3,ij)} = i(\phi^\dagger \tau^I D_\mu \phi)(\bar{q}_{Li} \gamma^\mu \tau^I q_{Lj}), \tag{2a}$$

$$O_{\phi\phi}^{ij} = i(\tilde{\phi}^\dagger D_\mu \phi)(\bar{u}_{Ri} \gamma^\mu d_{Rj}), \tag{2b}$$

$$O_{uW}^{ij} = (\bar{q}_{Li} \sigma^{\mu\nu} \tau^I u_{Rj}) \tilde{\phi} W_{\mu\nu}^I, \tag{2c}$$

$$O_{dW}^{ij} = (\bar{q}_{Li} \sigma^{\mu\nu} \tau^I d_{Rj}) \phi W_{\mu\nu}^I, \tag{2d}$$

$$O_{qW}^{ij} = (\bar{q}_{Li} \gamma^\mu \tau^I D^\nu q_{Lj}) W_{\mu\nu}^I, \tag{2e}$$

with generation indices i, $j = 1, 2, 3$ and the non-Abelian **SU(2)**$_L$ field strength components

$$W_{\mu\nu}^I = \partial_\mu W_\nu^I - \partial_\nu W_\mu^I - g\varepsilon_{IJK} W_\mu^J W_\nu^K \tag{3}$$

to be contracted with the Pauli matrices τ^I ($I = 1, 2, 3$). The $q_{L(R)i}$ are left(right)-handed quark spinors in the electroweak isodoublet (isosinglet) representation, and ϕ is the isodoublet complex SM scalar field acquiring a vacuum expectation value $\langle \phi \rangle = \frac{1}{\sqrt{2}}(0, v)^T$, and $\tilde{\phi} = i\tau^2 \phi^*$. Of the other electroweak operators listed in Ref. [28], $O_{\phi q}^{(1,ij)}$ and $O_{\phi u}^{ij}$ as well as all those containing the hypercharge field strength $B_{\mu\nu}$ only contribute to NC interactions, whereas the operators O_{Du}^{ij}, $O_{\tilde{D}u}^{ij}$, O_{Dd}^{ij} and $O_{\tilde{D}d}^{ij}$ appear to contribute to the tbW vertex. However, the differences $O_{Du(d)}^{ij} - O_{\tilde{D}u(d)}^{ij}$ are entirely redundant as is shown in Ref. [28], and the sums $O_{Du(d)}^{ij} + O_{\tilde{D}u(d)}^{ij}$ are proportional to the gauge boson momentum $q^\mu = (p_i - p_j)^\mu$ so that amplitudes containing these vertices vanish either for physical on-shell W or for on-shell light fermions coupling to the W, which is always the case at parton level for all processes to be considered for single top and top decay studies discussed here. So Eq. (2) represents the most general $d = 6$ operator basis generating anomalous tbW couplings, in which we shall therefore be complete in our phenomenological studies.

We could now straightforwardly begin to find and implement all interactions generated by the operator basis which could appear in the relevant amplitudes. However, this can become a rather involved business particularly for O_{qW}^{ij} which contains, apart from the trilinear coupling, also some relevant quartic terms such as e.g., $tbWg$ with a complicated Dirac and momentum structure. Therefore, in order to facilitate the implementation work we rather

follow the operator rewriting procedure of Ref. [28], illustrating the main steps here for O_{qW}^{ij}: starting from its decomposition into Hermitian and anti-Hermitian parts, the Hermitian part becomes

$$\frac{1}{2}[O_{qW}^{ij} + (O_{qW}^{ji})^\dagger] = \frac{1}{2}(\bar{q}_{Li} \gamma^\mu \tau^I q_{Lj})(D^\nu W_{\nu\mu})^I \tag{4}$$

(dropping the total derivative), where the EOM of the W field

$$(D^\nu W_{\nu\mu})^I = g\left\{ \bar{\ell}_{Li} \gamma^\mu \frac{\tau^I}{2} \ell_{Li} + \bar{q}_{Li} \gamma^\mu \frac{\tau^I}{2} q_{Li} \right.$$
$$\left. + i\left[\phi^\dagger \frac{\tau^I}{2} D^\mu \phi - (D^\mu \phi^\dagger) \frac{\tau^I}{2} \phi \right] \right\} \tag{5}$$

can be applied to replace the derivative. On the other hand, with some algebra [20,28] the anti-Hermitian part can be brought in the form

$$\frac{1}{2}[O_{qW}^{ij} - (O_{qW}^{ji})^\dagger] = -\frac{1}{4}(\bar{q}_{Li} \sigma^{\mu\nu} \tau^I i\overleftrightarrow{D} q_{Lj} W_{\mu\nu}^I - \text{H.c.}) \tag{6}$$

up to total derivatives, where the EOM of the quark field

$$i\overleftrightarrow{D} q_{Li} = Y_{ij}^u u_{Rj} \tilde{\phi} + Y_{ij}^d d_{Rj} \phi \tag{7}$$

(introducing Yukawa matrices $Y^{u/d}$) can be inserted. Putting it all together, one arrives at the operator equality

$$O_{qW}^{ij} = +\frac{g}{4}(\bar{q}_{Li} \gamma^\mu \tau^I q_{Lj})[(\bar{\ell}_{Lk} \gamma_\mu \tau^I \ell_{Lk}) + (\bar{q}_{Lk} \gamma_\mu \tau^I q_{Lk})] \tag{8a}$$

$$+\frac{g}{4}[O_{\phi q}^{(3,ij)} + (O_{\phi q}^{(3,ji)})^\dagger] \tag{8b}$$

$$-\frac{1}{4}[Y_{jk}^u O_{uW}^{ik} + Y_{jk}^d O_{dW}^{ik} - Y_{ki}^{u\dagger}(O_{uW}^{jk})^\dagger - Y_{ki}^{d\dagger}(O_{dW}^{jk})^\dagger]. \tag{8c}$$

Obviously, the terms in (8b) and (8c) are redundant and can be absorbed into the operators (2a)–(2d), whereas (8a) generates four-fermion contact interactions.

Although it is clear that without further restrictions there is enough freedom within the operator basis to independently vary all the couplings emerging from (2a)–(2d) and the associated contact terms coming from the rewriting (8), the rewriting procedure corresponds to a shift of the original operator coefficients. Setting $i = j = 3$ and dropping all generation superscripts from now on, these shifts are

$$\delta \operatorname{Re} C_{\phi q}^{(3)} = \frac{g}{2} \operatorname{Re} C_{qW}, \qquad \delta \operatorname{Im} C_{uW} = -\frac{m_t}{\sqrt{2}v} \operatorname{Im} C_{qW},$$
$$\delta \operatorname{Im} C_{dW} = -\frac{m_b}{\sqrt{2}v} \operatorname{Im} C_{qW} \simeq 0, \tag{9}$$

assuming an approximate decoupling of the third generation in the Yukawa matrices. With this setup, we can now go on to physical states of the gauge and matter fields and write down the interaction terms generated by our operator basis.

B. Parametrization of anomalous
charged-current couplings

Inserting the scalar vacuum expectation value and physical states of the gauge fields into the operators (2) and forming Hermitian combinations $C_x O_x + C_x^* O_x^\dagger$, one finds various trilinear interaction terms tbW, ttZ, ttA but also bbZ and bbA, as well as associated quartic interactions $ttWW$, $bbWW$, $tbWZ$, and $tbWA$ which are all necessary to maintain gauge invariance in the resulting amplitudes and have therefore been included in our implementation. The resulting effective tbW interaction Lagrangian can be written as

$$\mathcal{L}_{tbW} = -\frac{g}{\sqrt{2}} \bar{b} \gamma^\mu (V_L P_L + V_R P_R) t W_\mu^- + \text{H.c.} \tag{10a}$$

$$-\frac{g}{\sqrt{2}} \bar{b} \frac{i\sigma^{\mu\nu} q_\nu}{m_W} (g_L P_L + g_R P_R) t W_\mu^- + \text{H.c.} \tag{10b}$$

$$-\frac{g}{\sqrt{2}} \bar{b} \gamma^\mu \frac{q^2 - m_W^2}{m_W^2} (V_L^{\text{off}} P_L) t W_\mu^- + \text{H.c.}, \tag{10c}$$

where all couplings except for $V_L \equiv V_{tb} \simeq 1$ vanish in the SM at tree level, and get the following anomalous contributions from operator coefficients[2]:

$$\delta V_L = \left(C_{\phi q}^{(3)*} + \frac{g}{2} \operatorname{Re} C_{qW} \right) \frac{v^2}{\Lambda^2},$$

$$\delta g_L = \sqrt{2} C_{dW}^* \frac{v^2}{\Lambda^2},$$

$$\delta V_R = \frac{1}{2} C_{\phi\phi}^* \frac{v^2}{\Lambda^2}, \tag{11}$$

$$\delta g_R = \sqrt{2} C_{uW} \frac{v^2}{\Lambda^2},$$

$$\delta V_L^{\text{off}} = \frac{g}{2} \operatorname{Re} C_{qW} \frac{v^2}{\Lambda^2}.$$

The interaction terms (10a) and (10b) represent the on-shell parametrization widely used in various phenomenological studies (normalization convention taken from Ref. [28]), which is retrieved from the operators (2a)–(2d). The interaction (10c) emerges from the Hermitian part of O_{qW},

$$O_{qW} + O_{qW}^\dagger = (\bar{q}_{L3} \gamma^\mu \tau^I q_{L3})(\partial^2 W_\mu^I)$$

$$+ \text{ higher contact interactions}, \tag{12}$$

cf. Eq. (4), which—unlike the anti-Hermitian part—cannot be completely recast into a combination of the other four operators. However, the *partial* redundance of O_{qW} has been made explicit in the parametrization (10) by defining its on-shell part into V_L so that any contribution $\sim V_L^{\text{off}}$ vanishes when the W goes on the mass shell. Hence it is no surprise

that in δV_L of Eq. (11) we find again the shift of the coefficient $C_{\phi q}^{(3)}$ already stated in Eq. (9) after the operator rewriting. Furthermore, by comparison to Eq. (8), one finds that all contributions $\sim V_L^{\text{off}}$ must be in one-to-one correspondence to the four-fermion contact interactions given in (8a), which is also highlighted by the fact that in physical amplitudes the kinematic structure of the W propagator is exactly canceled by the q-dependent vertex.

We have now isolated the nonredundant contribution of O_{qW} to the tbW interaction Lagrangian, and also identified the most convenient way to implement it in a gauge-invariant way, namely by adding the quartic fermion vertices

$$\Delta\mathcal{L} = \frac{g_\times}{\Lambda^2} (\bar{b} \gamma^\mu P_L t)[(\bar{u}_k \gamma_\mu P_L d_k) + (\bar{\nu}_k \gamma_\mu P_L e_k)] + \text{H.c.}$$

$$\text{with} \quad g_\times = g \operatorname{Re} C_{qW} \tag{13}$$

(cf. Refs. [30,49,50]), giving a relation of coefficients

$$V_L^{\text{off}} = \frac{v^2}{2\Lambda^2} g_\times. \tag{14}$$

Of course, one might ask at this point if such a coupling structure should be counted among the anomalous tbW sector, but then again it must be noted that as a consequence of the common operator basis, the trilinear couplings are related to V_L^{off} through the underlying operator coefficients. Specifically, Eq. (11) illustrates that a limit on δV_L cannot be unambiguously mapped onto a limit on the operator coefficient $C_{\phi q}^{(3)}$ without also bounding δV_L^{off} (or the anomalous NC sector, see below). Moreover, the operator basis (2) and the corresponding set of couplings (10) parametrize *all* anomalous diagram insertions which can interfere with the SM diagram in a minimal way, making this approach consistent at the amplitude level. Finally, as pointed out in Sec. III C, the inclusion of the additional coupling also affects the interpretation of current and upcoming experimental results at the LHC.

Before moving on to the phenomenological implications, let us discuss briefly the issue of anomalous bottom couplings within the effective theory approach: since the original effective operators by construction respect the full electroweak gauge symmetry $\mathbf{SU}(2)_L \times \mathbf{U}(1)_Y$, it is no surprise to find certain relations within the set of anomalous electroweak couplings of the heavy doublet (t, b) after spontaneous symmetry breaking. For example, an anomalous CC contribution δV_L is directly related to the anomalous left-handed NC vector couplings ttZ and bbZ, the latter one stringently constrained by LEP data, so turning on δV_L while respecting all existing bounds necessarily implies a nonvanishing anomalous contribution to the left-handed ttZ vector coupling [28,51], or a fine-tuned relation with δV_L^{off}, cf. Eq. (11). Similarly, δg_R is directly related to the anomalous $ttZ/tt\gamma$ tensor couplings, just like δg_L is to the $bbZ/bb\gamma$ ones (cf. e.g., Refs. [28,52] for details).

---

[2]Note that in Eq. (37) of Ref. [28] the operator coefficient $C_{\phi\phi}^{33}$ appearing in δV_R should also be complex conjugated.

In short, it is impossible to vary the anomalous CC couplings in a consistent way within the effective operator approach without either getting anomalous NC couplings or including additional operators to fine-tune these effects away. Although these relations basically have no effect on a purely CC single top study, one should bear them in mind when addressing anomalous CC couplings (the WHIZARD implementation contains the option to automatically enforce these relations).

III. LHC PHENOMENOLOGY

Apart from indirect searches using low-energy observables, e.g., in flavor physics [53–55] or SM precision observables [56], there are basically two different classes of direct observables for top quark properties at the current collider experiments, namely those related to top production or top decays. While it is clear that only a combination of all available observables will deliver the best bounds on anomalous contributions, it is crucial to understand each analysis separately before the combination step. Therefore, we will focus here on the discussion of single top production cross sections, citing and using results from top decay studies to derive estimates for the most stringent bounds on the full anomalous parameter space at the end of the article.

Single tops are produced at the LHC (and Tevatron) in three different channels, namely s channel tb production, t channel tj production (where j denotes a light hadronic jet), and associated tW production, cf. Fig. 1. While experimentalists are struggling to identify and discriminate these channels at the detector level with suitable selection criteria, the theoretical question is how the corresponding measured cross sections σ_i^{det} (for final states $i = tb$, tj, tW) are represented as functions on the anomalous parameter space, i.e., how the measurement can be converted into bounds on the parameters. In this respect, a first step may be to separate the detector response from the hard production cross section

$$\sigma_i^{\text{det}}(\vec{g}) = \sum_j \varepsilon_{ij} \cdot \sigma_j^{\text{part}}(\vec{g}), \qquad (15)$$

summing over partonic production processes j as functions of the parameter point $\vec{g}$. ε_{ij} denotes the detector efficiency matrix mapping the process j onto the final state selection i, which can be retrieved with a detector simulation. Once the functions $\sigma_i^{\text{part}}(\vec{g})$ are known, experimentally measured

confidence intervals for σ_i^{det} can be mapped onto confidence intervals for $\vec{g}$ by formal inversion of Eq. (15).

However, the remaining question to be addressed in this approach is, where did we put the detector acceptance Φ, into ε or into σ_i^{part}? The significance of this question is obvious, since anomalous couplings might very well affect the differential distributions, thus making Φ a function of $\vec{g}$. Therefore, the answer to that question influences the strategy as well as the efforts necessary to compute the function $\sigma_i^{\text{part}}(\vec{g})$, and potentially also the bounds derived from it, as we will show in the following section.

A. Technical setup

1. Kinematics in the on-shell limit

The simplest approach is to neglect the $\vec{g}$ dependence of the acceptance entirely and pull it into ε, implying that the $\sigma_i^{\text{part}}(\vec{g})$ in Eq. (15) represent the set of total partonic cross sections integrated over the full phase space. Further neglecting finite width and interference effects with irreducible backgrounds enables one to decompose $\sigma_i^{\text{part}}(\vec{g})$ as

$$\sigma_i^{\text{part}}(\vec{g}) = \sigma_i^{\text{prod}}(\vec{g}) \times \prod \mathcal{BR}, \qquad (16)$$

where $\sigma_i^{\text{prod}}(\vec{g})$ denotes the full on-shell single top production cross sections, and the product of branching ratios accounts for the decays of the heavy particles, namely t and one or two Ws, depending on the production channel. Since all the on-shell production diagrams can contain only one anomalous tbW vertex insertion, it is argued in Ref. [37] that $\sigma_i^{\text{prod}}(\vec{g})$ may be written as a polynomial up to second order in $\vec{g}$,

$$\sigma_i^{\text{prod}}(\vec{g}) = \sigma_i^{\text{SM}} \sum_{k,l} \kappa_{kl}^i g_k g_l, \qquad (17)$$

where the σ_i^{SM} are the total SM cross sections, and the κ_{kl}^i denote the integrated products of diagrams with one insertion of g_k and g_l each, normalized to the SM point in each production channel i. Plugging (16) and (17) into (15), one arrives at the ansatz employed in Ref. [37],

$$\sigma_i^{\text{det}}(\vec{g}) = \sum_{j,k,l} \Big[\varepsilon \times \prod \mathcal{BR} \Big]_{ij} \cdot \sigma_j^{\text{SM}} \cdot \kappa_{kl}^j g_k g_l$$

$$\equiv \sum_{j,k,l} \varepsilon_{ij} \cdot \sigma_j^{\text{SM}} \cdot \kappa_{kl}^j g_k g_l. \qquad (18)$$

For brevity, this will be referred to as *on-shell approach* from here on. The advantage of the formula is obvious:
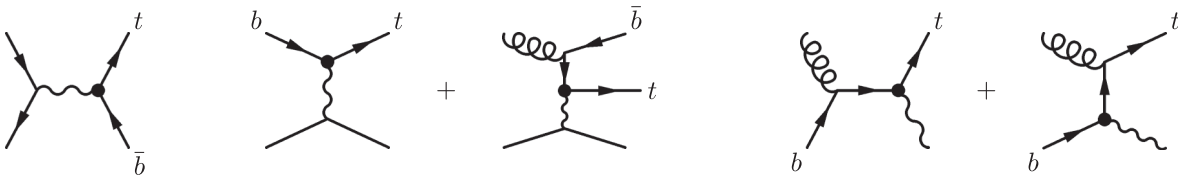
FIG. 1. Diagrams contributing to LO on-shell single top production (anomalous tbW vertex marked by a dot): s channel tb production (left diagram), t channel $tj + tbj$ production (center diagrams) and associated tW production (right diagrams).

once ε and the constant κs are known, the conversion of measured results into bounds on $\vec{g}$ becomes very simple and efficient. However, the validity of the assumptions leading to this result shall be addressed now.

2. Full matrix elements and acceptances including anomalous couplings

Equation (18) tells us that one should be able to vary the coupling point $\vec{g}$ within the ranges relevant for the study, with only minor effects on the detector response ε in the phase space window which corresponds to a given final state selection. However, Eq. (18) implies even more, namely that retrieving the matrix element response as a function of $\vec{g}$ and applying acceptance cuts on the phase space should approximately commute, or equivalently, Eq. (18) should give the same results as e.g.,

$$\sigma_i^{\text{det}}(\vec{g}) = \sum_j \varepsilon'_{ij} \cdot [\Phi^{\text{part}} \times \sigma^{\text{part}}]_j(\vec{g}), \qquad (19)$$

where the basic detector acceptance cuts such as p_T and η cuts on the partons and leptons, represented by Φ^{part}, are applied directly to the phase space integration and hence formally included in the $\vec{g}$-dependent part of the formula, while the matrix ε', assumed to be constant in $\vec{g}$, denotes the efficiency of mapping the partonic final states *at the acceptance level* Φ^{part} onto the final state selections at detector level.

To be more explicit, the idea is to accommodate as much of the acceptance cuts as possible within the $\vec{g}$-dependent part without becoming exclusive to any of the different final state selections, which are still contained in the $\vec{g}$-independent ε'. This obviously implies that the phase space window covered by ε' must be fully contained within the acceptance window Φ^{part}, leading to the notion that partonic acceptance and final state selection cuts should be adapted to each other as closely as possible.

Assuming leptonic t decay, we therefore apply the following acceptance cuts on the partonic phase space integration:

$$\Phi^{\text{part}}: \quad p_T(\ell, \nu) > 25 \text{ GeV} \quad \text{and} \quad |\eta(\ell)| < 3, \quad (20a)$$

$$p_T(j, b) > 30 \text{ GeV} \quad \text{and} \quad |\eta(j, b)| < 5, \quad (20b)$$

$$150 \text{ GeV} < m_{b\ell\nu} < 225 \text{ GeV}, \quad (20c)$$

where Eq. (20b) is required for only one of the two bs in the tbj process to be inclusive,[3] and all the cuts correspond to the detector-level selection criteria stated below.

Associated tW production is entirely omitted for the time being, because modeling this process within its detector acceptance window while at the same time remaining

inclusive with respect to the other processes is highly non-trivial, and only marginally affects our following statements (the main effect being the neglected contamination of the other final states at the detector level, which amounts to $\lesssim 10\%$ in the tb channel and practically vanishes in the dominant tj channel).[4] Clearly, this is still not the fully correct answer at detector level, but it should be closer to the truth than entirely neglecting the $\vec{g}$ dependence of ε, and the consistency of the two approaches can be checked.

Although it is clear that the object $[\Phi^{\text{part}} \times \sigma^{\text{part}}]_i(\vec{g})$ to be computed is much harder to handle than the constant κs (even more so if the full matrix element response including all off-shell and interference effects is to be taken into account), it is basically just a technical issue which can be tackled with appropriate Monte Carlo machinery and respective CPU time. For brevity, we will refer to this approach as *full matrix element (ME) approach* from now on. In the following section, we compare the results of Eq. (18) and (19), and see if the effort is justified.

B. Comparison of the results in the on-shell limit with the full results

For the measurement of the total cross section of a given final state at the detector level, the experimental sensitivity is given in terms of a measure for $\Delta\sigma/\sigma$, where estimations for total uncertainties are adopted from Ref. [37] for consistency, amounting to 20.8% (tb sel.) and 13.5% (tj sel.) for 10 fb^{-1} of LHC data at $\sqrt{s} = 14$ TeV. Therefore, we separate the overall normalization, which is basically given by higher-order SM results for the total production cross sections, from the modeling of the normalized LO matrix element response as a function of the anomalous coupling set $\vec{g}$, i.e., the κ_{on} coefficients in the on-shell approach or, more generally, a function $\Delta\sigma/\sigma(\vec{g}) \equiv \kappa(\vec{g})$ for each partonic input process i, where

$$\text{on-shell:} \quad \kappa_{\text{on}}^i(\vec{g}) = \sum_{k,l} \kappa^i_{kl} g_k g_l, \quad (21a)$$

$$\text{full ME:} \quad \kappa_{\text{full}}^i(\vec{g}) = \frac{[\Phi^{\text{part}} \times \sigma^{\text{part}}]_i(\vec{g})}{[\Phi^{\text{part}} \times \sigma^{\text{part}}]_i|_{\text{SM}}}, \quad (21b)$$

cf. Eqs. (18) and (19). Since the aim is to accommodate *all* coupling dependence therein, it is fruitful to first set $\varepsilon \equiv 1$ and compare this function for the different approaches at the partonic level.

1. Partonic level

To be self-consistent, we essentially redo the analysis procedure presented in Ref. [37] for the on-shell approach,

---

[3]Clearly, for full inclusiveness one would have to entirely drop the distinction of light and b flavors at partonic level, but the actual chance of mistagging the light forward jet is negligible once the full event topology (cf. tj selection below) is taken into account.

[4]Moreover, the suppression of the huge irreducible $t\bar{t}$ background in the radiative correction diagram tWb still is a topic of vivid discussion (cf. Ref. [18]), a problem that, again, does not affect the main statements of this paper. Still, it is clear that in the end also this channel should be addressed and included in a complete study.

employing WHIZARD to compute the coefficients of κ_{on} as well as produce parton-level samples, which are then processed with PYTHIA and DELPHES to retrieve ε. The quadratic coefficients (i.e., $\sim g_i^2$) are obtained in each production channel, cf. Fig. 1, by separately setting each $g_i = 1$, integrating the total cross section for on-shell single top production and finally normalizing to the SM point ($V_L = 1$, $V_R = g_{L,R} = 0$). The interference terms are computed similarly, setting always two couplings to 1 and subtracting the quadratic parts from the result before normalizing to the SM. The implementation of the vertices and phase space integration has been checked by switching off the pdfs and comparing WHIZARD to analytical results. Using the pdfs and parameter setup quoted in Ref. [37], WHIZARD also reproduces the on-shell κ coefficients stated there within numerical uncertainties. For all further WHIZARD results, we set $m_t = 173.1$ GeV, $m_b = 4.2$ GeV, $m_W = 80.42$ GeV and choose CTEQ6L1 [57] for pdfs.

In the full ME approach, the matrix element response is modeled according to Eq. (21b) by applying the acceptance cuts Φ^{part}, Eq. (20), to the full partonic off-shell matrix elements. In this approach, taking all finite width and interference effects into account, it is *a priori* not clear that the function $\kappa_{\text{full}}(\vec{g})$ obeys a simple polynomial expansion in $\vec{g}$, so rather than assuming a specific functional form, we use the WHIZARD machinery to scan the entire 4-dimensional parameter space $\vec{g} = (V_L, V_R, g_L, g_R)$ (effects of V_L^{off} will be addressed separately in Sec. III C) within the relevant numerical ranges $0 < V_L < 1.2$, $-1.2 < V_R < 1.2$ and $-0.6 < g_{L,R} < 0.6$ (cf. Ref. [37]), also including the full dependence of the top width on the couplings $\Gamma_t(\vec{g})$. Since Γ_t has already been measured, the most recent bound from DØ being $\Gamma_t = 2.00^{+0.47}_{-0.43}$ GeV [58], it is included in our analysis as an additional observable.[5] The numerical results can then be used to test the validity of the polynomial parametrization, Eq. (21a), in the following way: the normalized matrix element response κ may always be expanded as

$$\kappa(\vec{g}) = \sum_i \kappa_1(g_i) + \sum_{i,j} \kappa_2(g_i, g_j) + \sum_{i,j,k} \kappa_3(g_i, g_j, g_k) + \dots,$$
(22)

---

[5]Clearly the experimental analysis performed in Ref. [58] to extract Γ_t from data will itself also be affected by $\vec{g}$-dependent acceptances as discussed in the course of this paper. However, since we do not aim at a reassessment of their analysis in this respect, yet also want to exclude regions in parameter space which are completely unphysical with respect to Γ_t, we still include the observable, inferring the $\Gamma_t(\vec{g})$ dependence over the full phase space. This approach is conservative, because our results indicate that including the full acceptance dependence generally tends to improve the sensitivities, cf. Fig. 4. *A posteriori*, we find that, due to the still large error bars, the current measurement of Γ_t constrains $\vec{g}$ much less than the cross sections. The limits on $\vec{g}$ would therefore not be affected substantially by such a reassessment.

where the κ_i are polynomials in their respective arguments. Offsets κ_0 from squared irreducible background diagrams could be considered, but are obviously independent of $\vec{g}$ and merely add to the background normalization, so we just subtract them from the scans, while keeping all interference effects (appearing as terms linear in the g_i in κ_1) for completeness. Usually this series terminates after κ_2, which becomes obvious when applying the narrow width approximation, where additional coupling effects cancel in the interplay of the decay vertex insertion, width dependence and phase space integration. This basically leads to the quadratic form in the on-shell approach. However, in the special case of single tops, production and decay are interrelated via the same set of CC couplings, thus affecting production as well as decay distributions, which in combination with the detector acceptance cuts might lead to deviations from the on-shell result in some regions of the parameter space.[6]

In order to estimate the size of the moments κ_3, in our cross section scans we consider 2-dimensional subplanes (g_i, g_j) among the anomalous couplings (V_R, g_L, g_R) for different fixed values of V_L. After subtracting all the lowest moments,

$$\Delta\kappa(\vec{g}) = \kappa(\vec{g}) - \sum_{k=i,j,V_L} \kappa_1(g_k) - \sum_{k=i,j} \kappa_2(g_k, V_L), \quad (23)$$

within the on-shell picture the remaining contribution $\Delta\kappa(\vec{g}) \sim \kappa_2(g_i, g_j)$ should then be independent of the value of V_L, otherwise it would, by definition, contain some $\kappa_3(g_i, g_j, V_L)$. For illustration, we choose the coupling subspace $(g_i, g_j) = (V_R, g_L)$, because it is one of the dominant interference contributions to all production processes. We then evaluate $\Delta\kappa|_{V_L=1.2} - \Delta\kappa|_{V_L=0.2}$. The resulting picture is mixed: while in the s channel the result is practically 0 over all the V_R-g_L plane, in the t channel process $\bar{t}j$, which plays a central role because of its comparably large cross section, this difference amounts to ~ -0.2 at $V_R \simeq \pm 1$ and $g_L \simeq \pm 0.5$ along the interference direction $V_R \sim 2g_L$ (cf. Fig. 2), which is of the same size as the respective on-shell contribution $\sim -0.5 \times V_R \times g_L$, (the same is true for the $V_L g_R$ interference in the tj channel). For comparison, we repeat the whole procedure selecting only the resonant single top diagrams for the scan (including the full top width dependence on $\vec{g}$), finding that background interference only plays a minor role.

Furthermore, note that there are other interference directions also showing substantial effects, e.g., in the g_L-g_R plane of the s channel, but the $V_R g_L$ interference is the most interesting one because it is large in all channels, and respective bounds are expected to remain rather weak also from other experiments along the considered direction

---

[6]Note that this is a qualitative difference to QCD (LHC) or NC (International Linear Collider) $t\bar{t}$ production, where production and decay are affected by different sets of anomalous couplings.
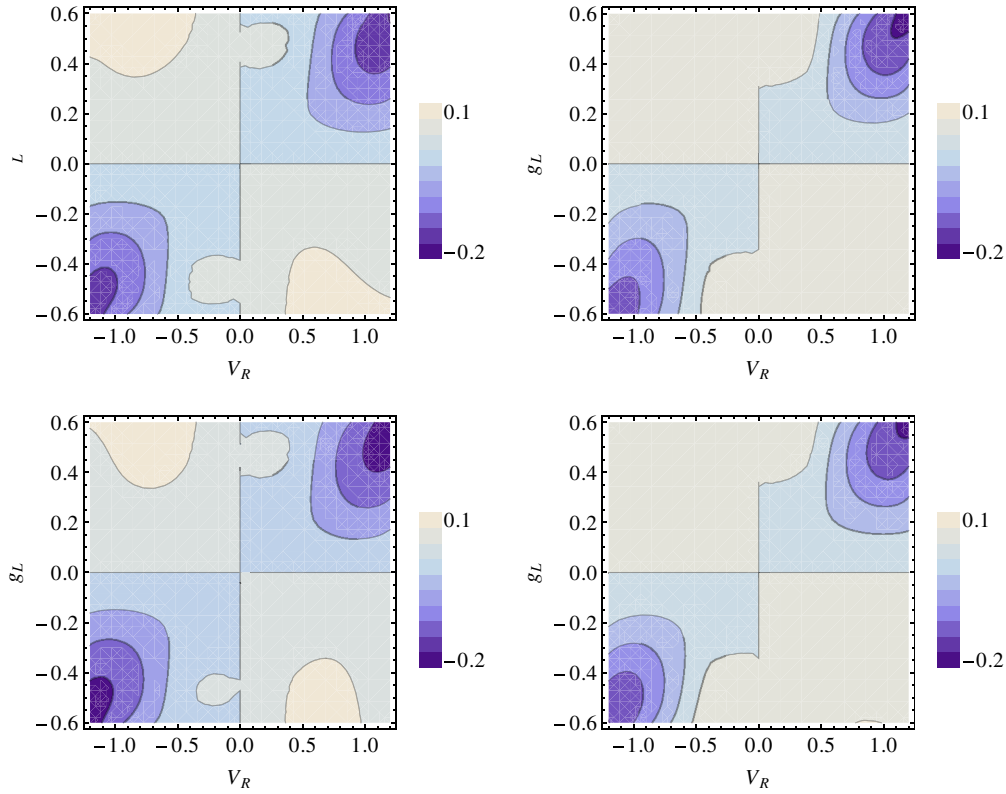
FIG. 2 (color online). $\Delta\kappa|_{V_L=1.2} - \Delta\kappa|_{V_L=0.2}$ in the $\bar{t}j$ process (left) and $\bar{t}bj$ process (right), based on full matrix elements (top) and resonant diagrams (bottom).

$V_R \sim 2g_L$ [37]. All in all, these numbers indicate strongly that the interference and off-shell effects contained in the full matrix elements might become important at the level of the coupling limits to be expected experimentally, at least in a stand-alone single top cross section study at the LHC, and should be checked in any case.

In order to further quantify this effect and exclude potential artifacts from unphysical regions in the parameter space, we now systematically scan the $V_R g_L$ interference along the direction $V_R \sim 2g_L$ as a function of V_L, including resonant off-shell diagrams for anomalous single top production and decay. We observe that the scans do show a quadratic dependence on V_R and g_L to a very good approximation at any value of V_L (cf. Fig. 3), so the respective coefficients $\kappa_{V_R} \sim V_R^2$, $\kappa_{g_L} \sim g_L^2$, and $\kappa_{V_R g_L} \sim V_R g_L$ can be extracted from quadratic fits along the axes V_R, g_L, and $V_R = 2_{g_L}$ for each fixed value of V_L and $g_R = 0$. This is done for the full phase space integration as well as for the acceptance region defined in Eq. (20). As illustrated in Fig. 4 for the t channel processes, when integrating over the full phase space the deviations from the on-shell result are very small as expected from the narrow width approximation, whereas application of the acceptance cuts leads to substantially different fit coefficients that also depend on the value of V_L.

Particularly this dependence of the magnitude of the $V_R g_L$ interference on V_L is an example for the breakdown

of the quadratic on-shell approach. However, this dependence is rather small in κ_{V_R} and κ_{g_L} which come with squares of the respective couplings and therefore dominate the sensitivity of a given process to these couplings, so it might still be a good approach to expand the full κ_{full} as a quadratic form in *small* anomalous deviations from the SM point $V_L = 1$, namely by choosing $V_L = 1$ as an origin. As explained before, the numerical values are extracted from quadratic fits to 1-dimensional coupling scans (including acceptance cuts) in all directions of $\vec{g}$, and all interference directions $g_i g_j$. A major difference to the original on-shell quadratic form is the appearance of large linear terms in the couplings, which now encode the interference with the SM. In Figs. 5 and 6, we compare the different quadratic parameterizations, namely, κ_{on} from the on-shell approach and κ_{fit} inferred from the fits, to the full ME response κ_{full}, illustrating two statements: First, κ_{on} significantly deviates from κ_{full} in various parts of the parameter space relevant to the analysis, particularly in the g_L-g_R and V_R-g_L planes. Second, although still neglecting the higher coupling dependences, κ_{fit} inferred from quadratic fits to the full scan does show a significantly improved agreement with the full scan while still being fast and efficient. This is further illustrated in Figs. 7 and 8 showing $\pm 1\sigma$ sensitivity contours around the SM strength $\kappa = 1$ for various anomalous coupling combinations and production processes: especially when the momentum-dependent couplings $g_{L,R}$ are
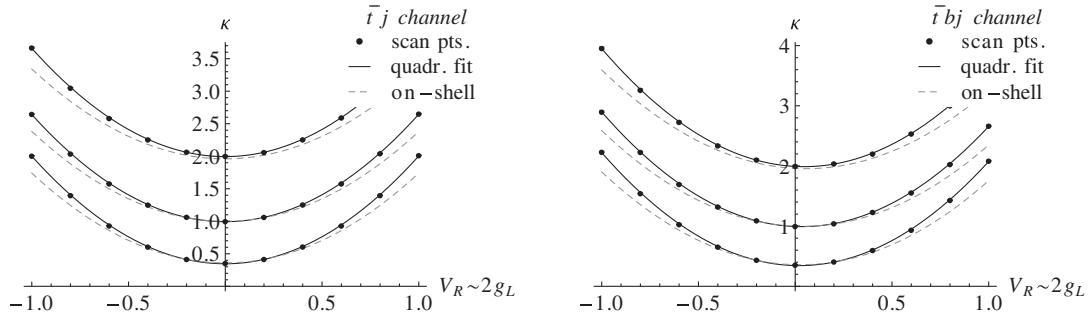
FIG. 3. κ scan results and quadratic fits of resonant matrix elements inside the acceptance region along the coupling direction $V_R \sim 2g_L$, for $V_L = 0.6$, 1.0 and 1.4 (bottom to top) in the $\bar{t}j$ channel (left) and the $\bar{t}bj$ channel (right). Grey dashed lines indicate the on-shell κ function.
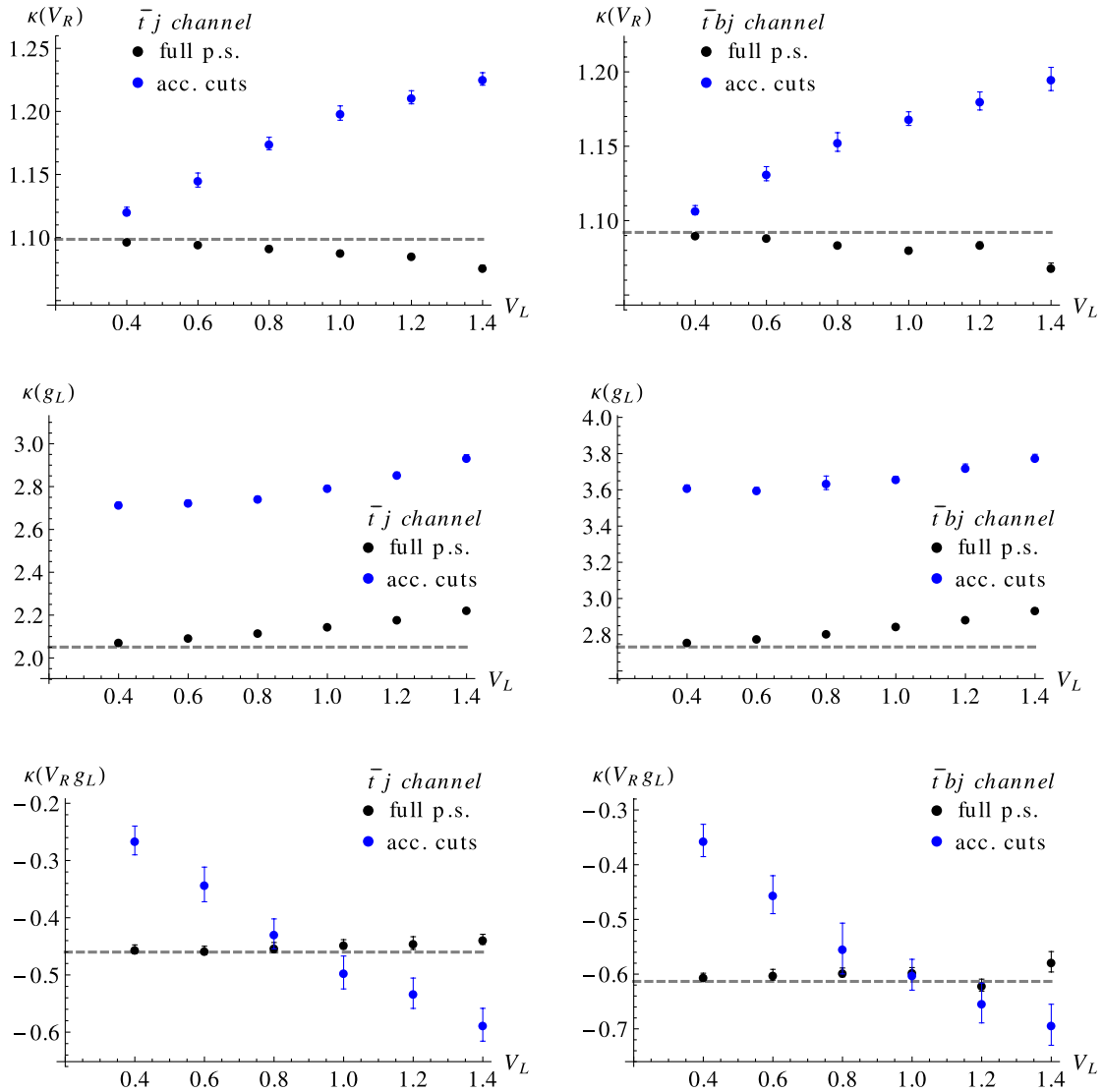
FIG. 4 (color online).   Numerical results for various κs in the processes $\bar{t}j$ (left) and $\bar{t}bj$ (right), as extracted from quadratic fits to the normalized cross sections. The dashed line indicates the value of the on-shell κ in each case.
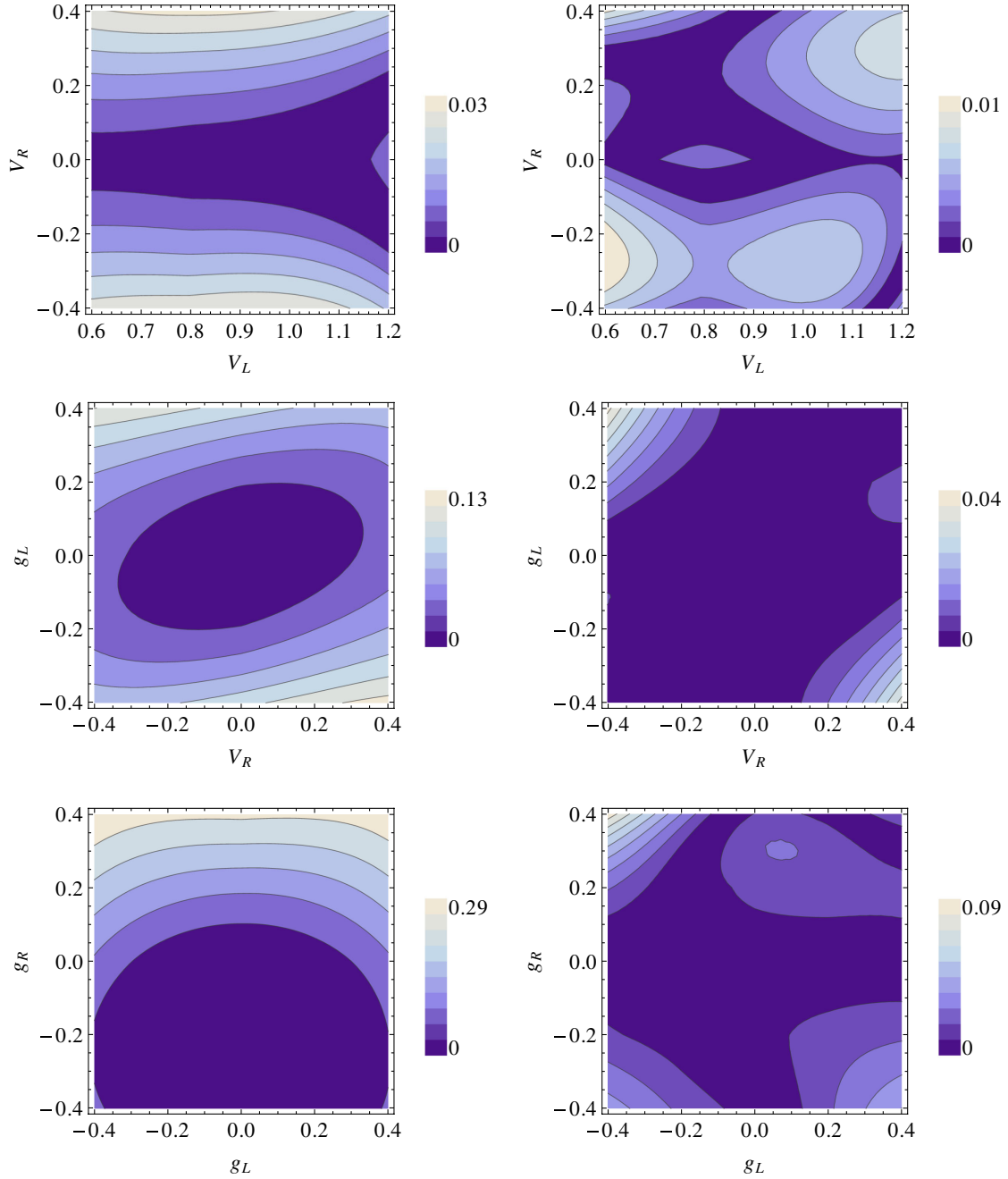
FIG. 5 (color online). The differences $|\kappa_{\text{full}} - \kappa_{\text{on}}|$ (left) and $|\kappa_{\text{full}} - \kappa_{\text{fit}}|$ (right) in various coupling planes of the $\bar{t}j$ process. Note that the heat scales on the left are of the size of the expected experimental sensitivity to the t channel ($\sim 13\%$), and significantly decrease on the right.

involved, there are remarkable shifts of the contours when going from the on-shell to the full ME approach, but generally these effects are modeled very well by the adapted quadratic parametrization $\kappa_{\text{fit}}(\vec{g})$, while the machine cost reduces from a 4D scan over $\vec{g}$ to a set of 1D scans along all axes g_i and interference directions $g_i g_j$ for each input process. We now go on to the detector level to quantify the impact of these different approaches on exclusion bounds on anomalous couplings from combined cross section measurements.

2. Detector level

In order to obtain a detector efficiency matrix in the various approaches, samples of $500\,k$ events are produced in each partonic production process, once integrating the full off-shell matrix elements over the acceptance region, Eq. (20), and once integrating the resonant matrix elements over the full phase space, letting the tops decay off-shell into a b quark, a charged lepton and a neutrino, analogously to Ref. [37]. All the parton-level samples are processed with PYTHIA and DELPHES to obtain events at
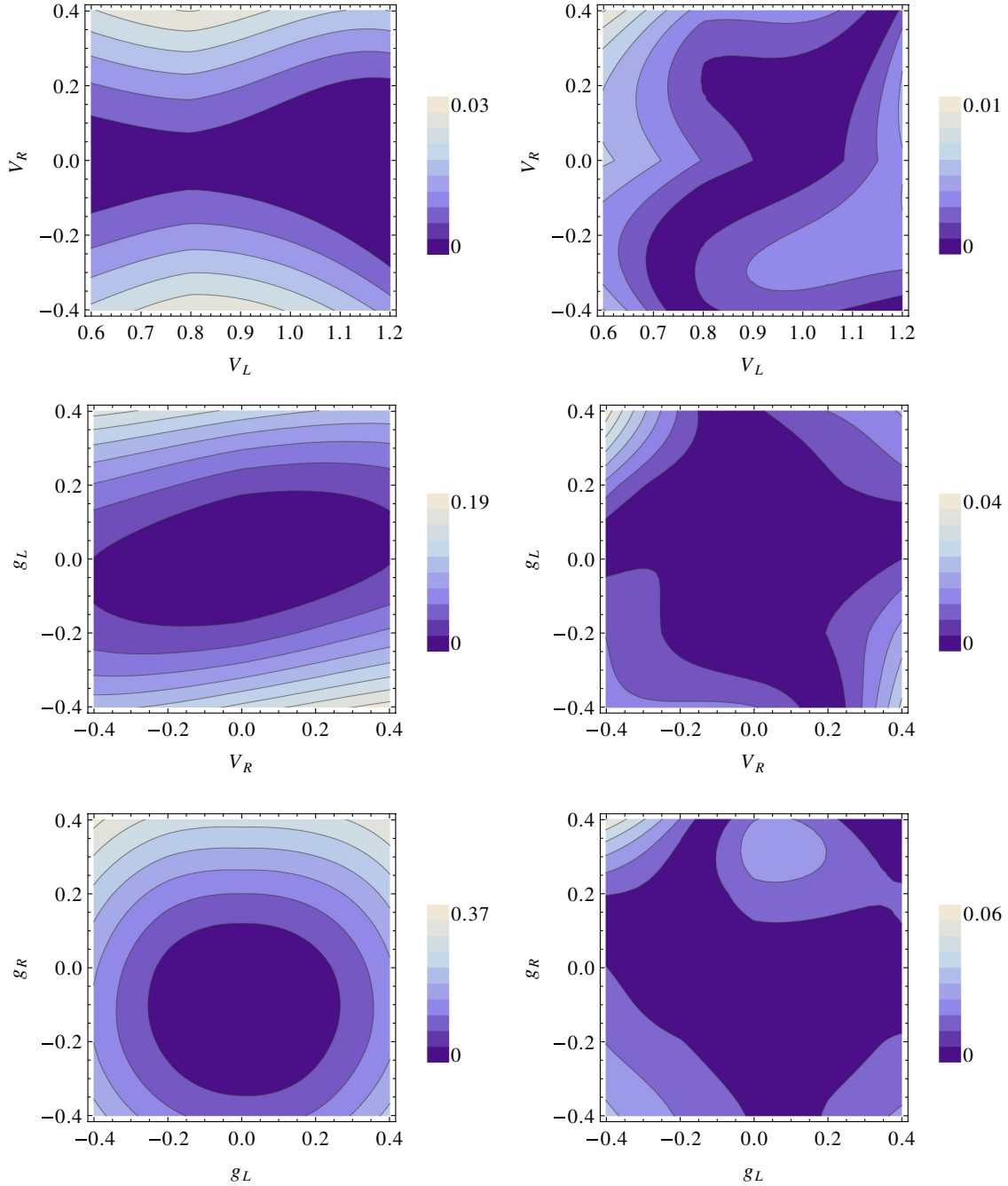
FIG. 6 (color online). The differences $|\kappa_{\text{full}} - \kappa_{\text{on}}|$ (left) and $|\kappa_{\text{full}} - \kappa_{\text{fit}}|$ (right) in various coupling planes of the $\bar{t}bj$ process (note the heat scales, cf. discussion in Fig. 5).

detector level. This is done for the SM point as well as the coupling configurations

$$
\begin{aligned}
&\text{A: } V_L = 1, \qquad V_R = 0.3, \qquad g_L = 0.15, \\
&\text{B: } V_L = 1, \qquad g_R = 0.024,
\end{aligned}
\tag{24}
$$

taken from Ref. [37] to facilitate comparison. Note that in each case a consistent top width $\Gamma_t(\vec{g})$ is calculated beforehand and the result checked to comply with experimental constraints [58]). Again for comparison reasons, we also

adopt the final state selection cuts stated in Ref. [37] which define the various components of ε: apart from requiring an isolated lepton (that is, e or μ) with $p_T > 25$ GeV and missing transverse energy $\not{E}_T > 25$ GeV, the selection criteria for the three final state signatures are, respectively

(1) For tb selection: exactly two b tagged jets (assuming a tagging efficiency of 0.6) with $p_T > 30$ GeV, and neither central nor forward light jets with $p_T > 15$ GeV. In addition, the top momentum p_t is reconstructed from one of the bs together with the
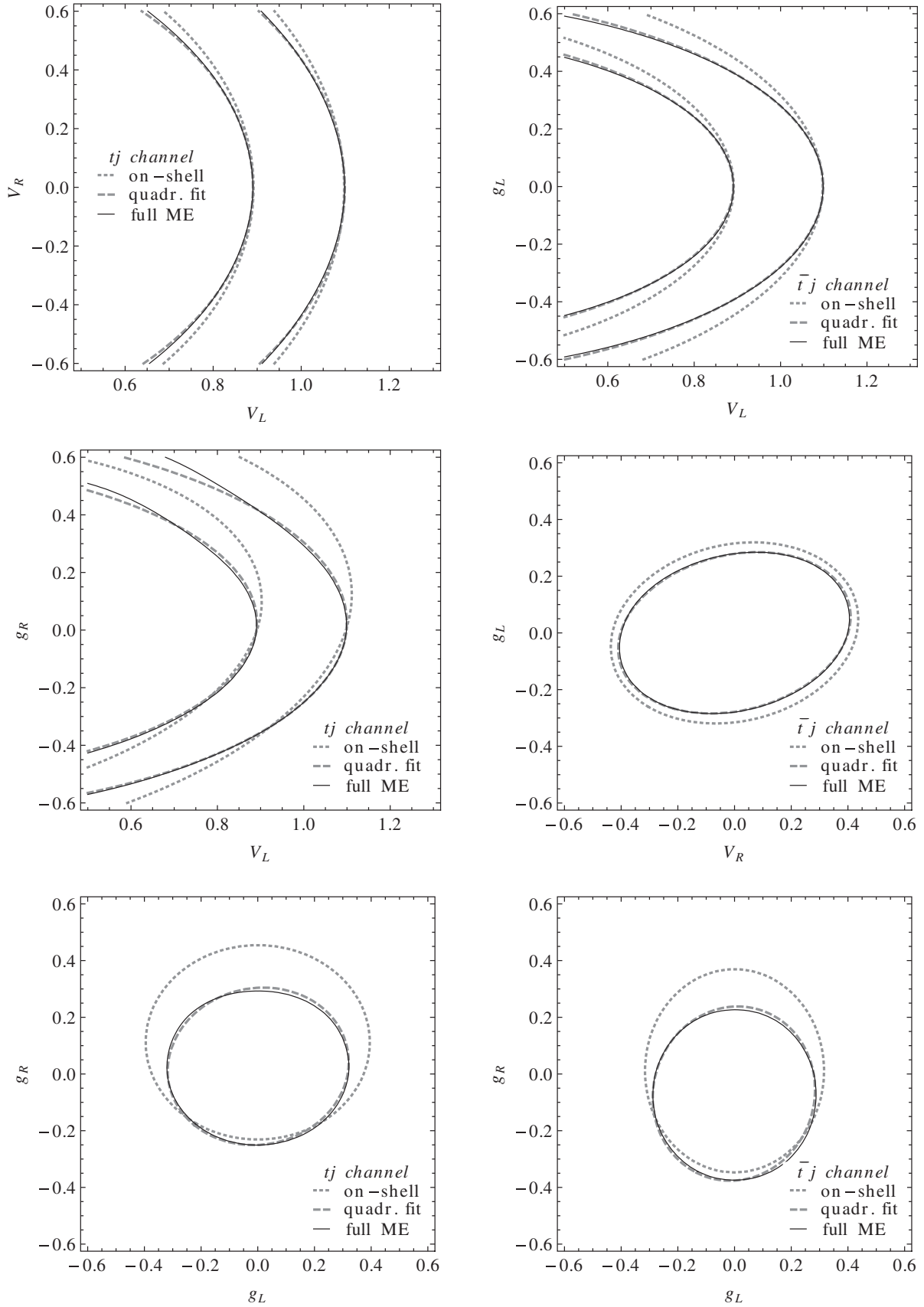
FIG. 7. Comparison of the 1σ contours for the various matrix element response functions κ_{on}, κ_{fit} and κ_{full} at parton level, for tj and $\bar{t}j$ production processes in different coupling planes (setting the others to their SM values).
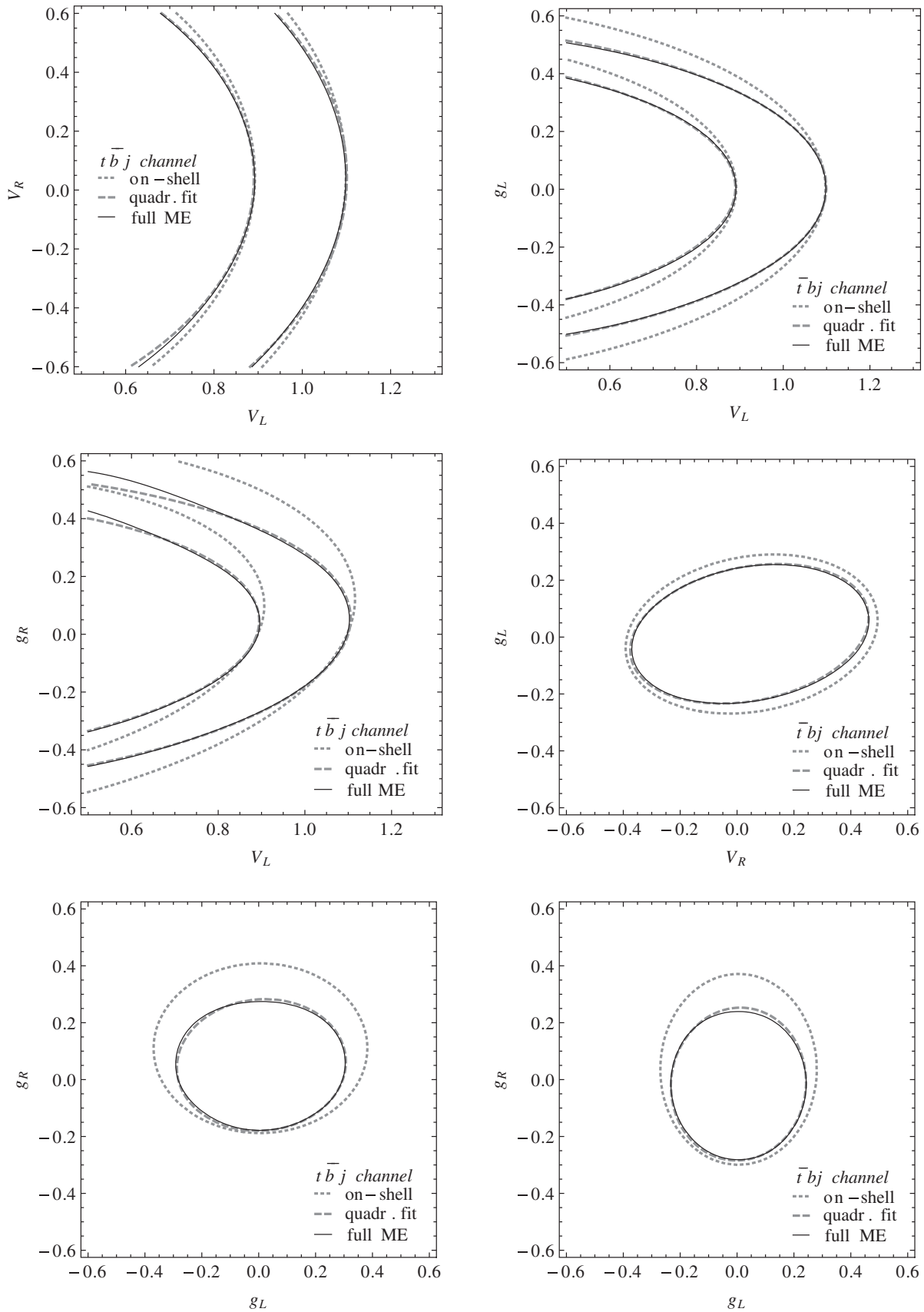
FIG. 8. Comparison of the 1σ contours for the various matrix element response functions $\kappa_{\rm on}$, $\kappa_{\rm fit}$ and $\kappa_{\rm full}$ at parton level, for $t\bar{b}j$ and $\bar{t}bj$ processes in different coupling planes (setting the others to their SM values).

charged lepton and $\not{E}_T$ (to be identified with the neutrino p_T), by applying the on-shell constraint $(p_\ell + p_\nu)^2 = m_W^2$ and picking the smaller of the two solutions for the longitudinal component of p_ν. Finally, the resulting top mass must lie between 150 and 225 GeV.

(2) For tj selection: at least one b jet with $p_T > 30$ GeV (one of them reconstructing p_t together with the leptons as explained above), one light forward jet with $p_T > 50$ GeV and $2.5 < |\eta| < 5$ and no more than one additional light central jet, which may have $p_T < 30$ GeV only.

By applying every final state selection to each of the $500\,k$ event samples corresponding to the partonic input processes and averaging over lepton flavors and charge states, we find for the samples from resonant diagrams integrated over the full phase space an efficiency matrix ε (in %) at the SM point,

$$
\begin{array}{c|ccc}
 & tb & tj & tbj \\
\hline
tb\ \text{sel.} & 0.658(6) & 0.040(1) & 0.051(2) \\
tj\ \text{sel.} & 0.165(3) & 0.647(6) & 0.531(5)
\end{array}. \qquad (25)
$$

For the full ME approach, we run the selection criteria described above on the detector level samples from full matrix elements integrated over the acceptance region, inferring ε' (in %)

$$
\begin{array}{c|ccc}
 & tb & tj & tbj \\
\hline
tb\ \text{sel.} & 1.28(1) & 0.039(1) & 0.031(1) \\
tj\ \text{sel.} & 0.282(4) & 1.52(1) & 1.023(7)
\end{array} \qquad (26)
$$

at the SM point.

Before moving on to detector-level coupling limits, the detector efficiency matrices can be compared between the various coupling points, Eq. (24), to test the assumption of a constant detector response. While the small admixture of g_R in point B only has a negligible effect on the efficiencies, we observe that there are sizable changes in the efficiencies when going from the SM point to point A, amounting to some 15% (8%) of the original values for tb (tj) selection in the samples with full phase space integration at parton level. However, when going close to the detector acceptance region already with the partonic input, this dependence is reduced to ~6% (4%), thus improving on another source of systematic uncertainty.

Taking approximate next-to-next-to-leading order on-shell s and t channel production cross sections from the literature [59,60] [multiplied by a partonic acceptance efficiency corresponding to the cuts in Eq. (20) in the full ME approach] to normalize the SM reference point for each input process, we now have all ingredients at hand to derive limits on $\vec{g}$ from a set of cross section measurements, modeled by Eqs. (18) and (19), and compare the results. In the t channel, the matrix element response for the detector-level analysis is modeled using only $t\bar{b}j$ and

$\bar{t}bj$ processes for simplicity, and because it was argued that the corresponding distributions already describe the proper next-to-leading order (NLO) behavior rather well [61,62]. Moreover, it was shown [63,64] that NLO corrections affect the differential distributions in s and t channel single top production only marginally, at the few % level, and can thus be readily accounted for by channel specific overall K factors, as in our analysis. A more comprehensive analysis including coupling-dependent K factors, similar to the case of anomalous flavor changing gluon couplings [65] and extending an existing study on anomalous top decays at NLO [66], will moderately influence the numerical values of the exclusion bounds. However, our results concerning the relative importance of the quartic couplings and the need to include the full matrix elements remain valid.

Now turning to the resulting bounds at the detector level, as already anticipated from the 1σ contours in Figs. 7 and 8 the effects on $V_{L,R}$ remain small in general, while the largest differences are found when the momentum-dependent couplings $g_{L,R}$ are involved, particularly in the g_L-g_R plane illustrated in Fig. 9. In this case, when single channels and charge states are considered separately, the different approaches tend to produce very different exclusion bounds. Figure 9 might also suggest that after combining all channels and considering the ratio $R(\bar{t}/t)$ of cross sections for t and $\bar{t}$ production in the t channel as an additional observable (tentatively assuming 2% statistical and 3% systematic uncertainty as estimated for 10 fb^{-1} at $\sqrt{s} = 14$ TeV in Ref. [37], in the absence of a more detailed experimental assessment), one might end up with the same exclusion limits again, but indeed this depends heavily on the total uncertainty of R in the actual experiment (cf. "R_2" in Fig. 9). In any case, when the aim is to properly understand and quantify the sensitivities to anomalous couplings of the various final states separately, going from the on-shell approach to full matrix element responses inside the selection acceptance region produces considerable effects that should not be neglected. In that respect, the adapted quadratic parametrization introduced above, employing quadratic fits to off-shell scans inside the acceptance region, represents a very good approximation to the full off-shell parameter scan (cf. Figs. 5–8).

C. Pinning down the off-shell coupling

After discussing the technical issue of modeling the LO matrix element response to anomalous top couplings at an experimentally relevant acceptance level, and validating an adapted quadratic parametrization which simultaneously meets the demands of machine efficiency and good agreement with the full off-shell coupling scan in the previous section, the closing section of the paper is devoted to the application of the new approach to a physical issue, namely a possible admixture of the additional anomalous coupling V_L^{off} introduced in Sec. II B, to the single top cross sections
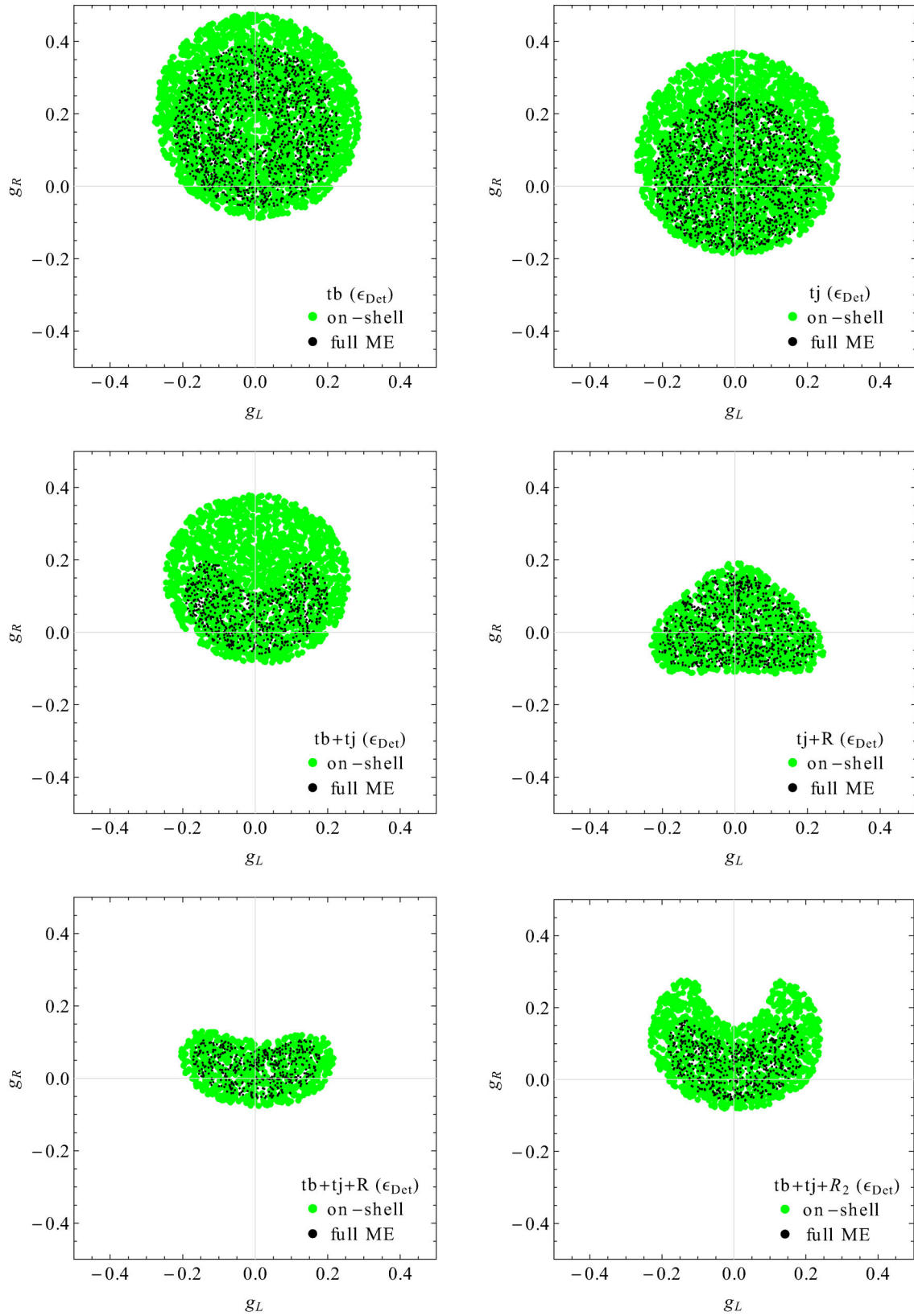
FIG. 9 (color online).   Combined 1σ limits on g_L and g_R ($V_L = 1$, $V_R = 0$) from single final states (top), combined final states (center left), and including the observable $R(\bar{t}/t)$ (center right and bottom). "R_2" denotes a factor 2 on the experimental resolution of R.
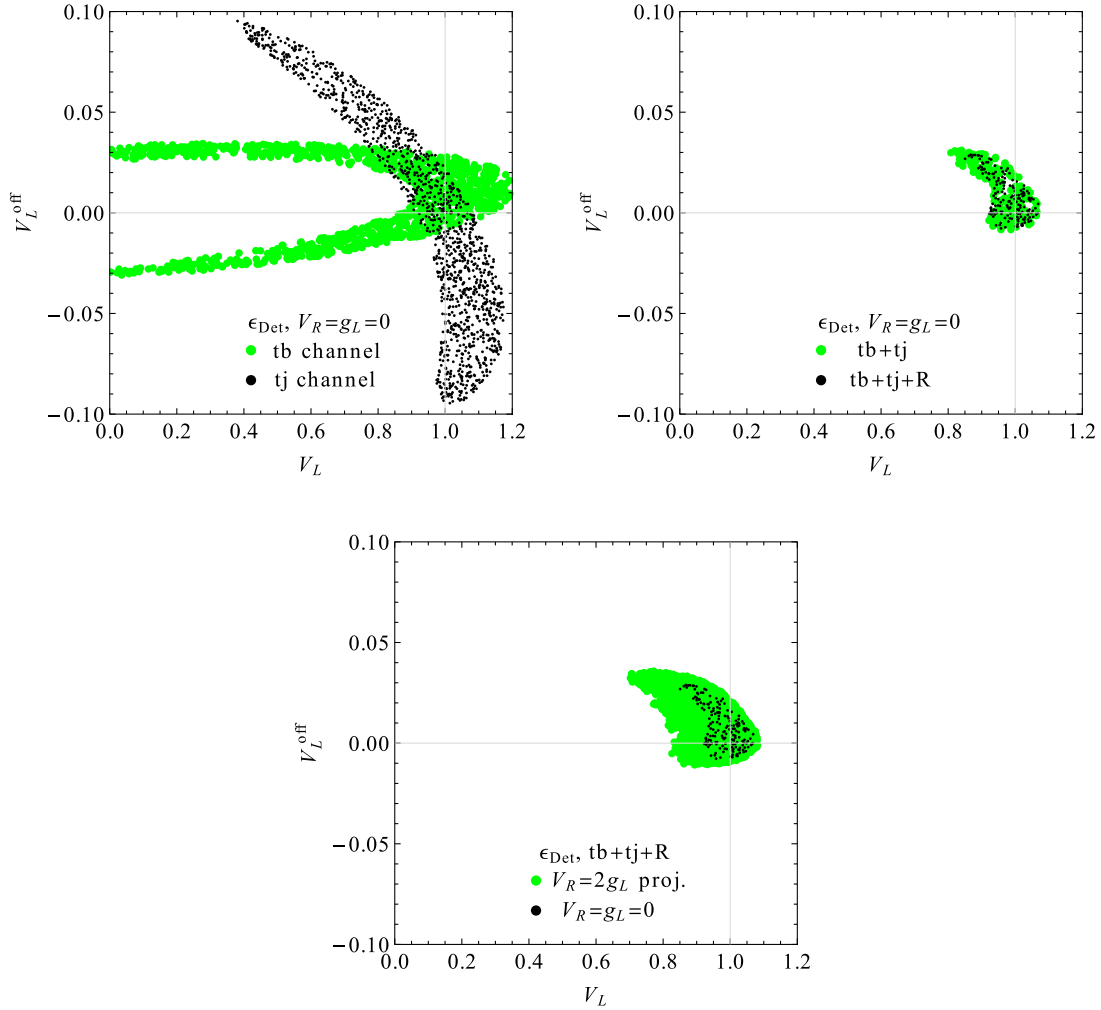
FIG. 10 (color online).   Combined 1σ contours in the V_L-V_L^{off} plane, setting $V_R = g_L = 0$ (top) or projecting over the direction $V_R = 2g_L$ (bottom).

(the total top width is also included as an observable, but its sensitivity to V_L^{off} is kinematically suppressed compared to the other anomalous couplings, since the relevant scale m_t is lower than $\sqrt{\hat{s}}$).

Considering the experimental sensitivities to the anomalous couplings of the total cross sections stated above for the LHC (which are already dominated by systematics), it is clear that a stand-alone study of single top cross sections alone will never provide the most stringent bounds on the complete parameter space of anomalous CC couplings, including V_L^{off} or not. Therefore, rather than just adding another direction to $\vec{g}$, the focus shall be directed here to those regions of the parameter space where single top cross sections actually become the crucial inputs to the combined limits.

More explicitly, the top decay observables (mostly related to the charged lepton distribution) are very sensitive to anomalous W helicity fractions generated by V_R, g_L and g_R (cf. Refs. [37,40,41,67]). For example, the limit $|g_R| \lesssim 0.024$ stated in Ref. [37] for our LHC reference point

(10 fb^{-1} at 14 TeV) is more than an order of magnitude below the sensitivity of the cross sections, so we may as well set $g_R \equiv 0$ for our purposes. On the other hand, the large interference among V_R and g_L leads to rather poor bounds $|V_R| \lesssim 0.3$, respectively, $|g_L| \lesssim 0.15$ as long as they are fine-tuned to $V_R \sim 2g_L$. Finally, since decay observables basically measure helicity fractions, they are sensitive to neither the overall vertex normalization nor to the admixture of V_L^{off} to the left-handed vector part. This is where the cross sections come into play, delivering the most stringent direct constraints. In Fig. 10, we therefore present combined limits on V_L and V_L^{off} from single top cross sections, both setting $V_R = g_L = 0$ as well as varying over $-0.3 \leq V_R = 2g_L \leq 0.3$. The very different sensitivities of the two final states greatly help in the combined limit: the s channel is very sensitive along V_L^{off} due to the kinematics, whereas the t channel basically cuts the substantial interference in the s channel along V_L. Still, the resulting limit on V_L deteriorates from $0.9 < V_L < 1.1$ ($V_L^{\text{off}} = 0$) to $0.82 < V_L < 1.1$ (V_L^{off} varied). Naturally,
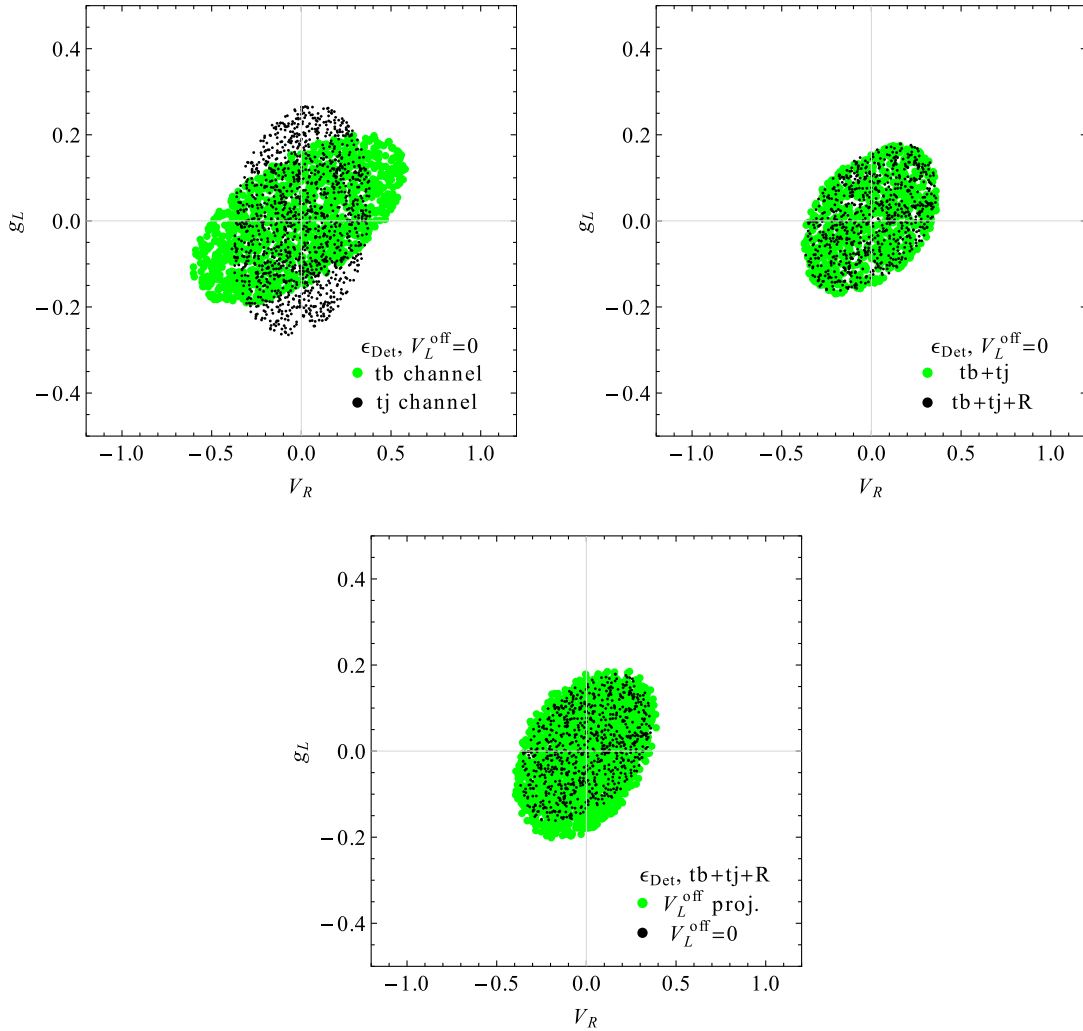
FIG. 11 (color online). Combined 1σ contours in the V_R-g_L plane, setting $V_L = 1$ and $V_L^{\mathrm{off}} = 0$ (top) or projecting (bottom).

projecting over the remaining freedom in V_R and g_L instead of switching them off further relaxes the combined limits to $0.68 < V_L < 1.1$. Figure 11 displays combined bounds in the V_R-g_L plane, switching off respectively varying over V_L^{off}.

In the long run, it is perfectly clear that this ambiguity among V_L and V_L^{off} remaining in the single top cross sections can be further resolved, namely by examining differential distributions, since V_L^{off} scales very differently with the partonic $\sqrt{s}$ than V_L. (In fact, V_L^{off} behaves like, or parameterizes, a heavy off-resonant new degree of freedom, cf. e.g., Ref. [68]). However, this issue will have to be tackled in the s channel where the momentum of the W propagator producing the top becomes timelike. Sensitive observables would obviously be the total invariant mass m_{tb} of the final state or the pseudorapidity η_b of the hard b jet produced along with the single top. However, such a study is experimentally challenging, since it requires a very good isolation of the tiny s channel signal from the huge t channel contamination, whereas at present this signal has

not even been established yet individually at the LHC (the most recent search being [69]). Hence, one should stay careful when stating limits on V_L from measurements of the overall size of V_{tb} until its kinematic behavior is further clarified experimentally.

IV. CONCLUSIONS

In this paper, we have revisited the model-independent parametrization of anomalous top couplings to SM gauge bosons within the effective operator approach, paying special attention to the charged-current sector and its phenomenological implications at current hadron colliders. More explicitly, addressing the minimal fully general set of anomalous trilinear tbW couplings coming from dimension six effective operators, there is a controversy regarding the meaning of "fully general," namely whether an off-shell interaction contained in the original operator basis should be dropped because it turns out to be related to four fermion contact interactions after application of the equations of motion, or not. While dropping it and sticking

to the usual coupling basis (V_L, V_R, g_L, g_R) naturally simplifies the analysis, there are good arguments to include it: since it emerges from the minimal gauge-invariant operator basis that also generates the trilinear couplings, the respective coupling size V_L^{off} is related to the other ones by the underlying operator coefficients. (For example, an experimental limit on δV_L is ambiguous in the context of effective operator coefficients, requiring knowledge about either δV_L^{off} or the NC sector to be resolved.) For the same reason, the coupling basis $(V_L, V_R, g_L, g_R, V_L^{\text{off}})$ parameterizes the complete set of anomalous diagrams which interfere with the SM diagram in a minimal way, so including it is also consistent at the level of matrix elements.

In the phenomenological part, the dependence of single top cross sections on anomalous tbW couplings in s and t channel production is examined, stressing the fact that the couplings do not only affect the total cross sections but also final state distributions, which determine the selection efficiencies within the detector acceptance region. While these effects are usually considered small, working with constant detector efficiencies and modeling the whole coupling dependence on the basis of on-shell production amplitudes, we use the WHIZARD machinery to scan the full off-shell matrix element dependence on the couplings inside the acceptance window defined by the final state selection cuts. Comparing to the on-shell approach, one finds considerable deviations in some regions of the parameter space, especially where the momentum-dependent couplings $g_{L,R}$ are involved, affecting the sensitivities of the various production channels to those couplings and therefore also the limits derived from the experiment. Finally, an adapted polynomial approach of the coupling dependence is discussed, which is based on quadratic fits to the full off-shell matrix element response including detector acceptance, and turns out to parametrize the full scan result rather well while still being fast and efficient. However, it is also stated as a result of the present study that the theoretical modeling of the coupling dependence should be adapted as closely as possible to a given experimental analysis with defined selection criteria to minimize the systematic uncertainty of the derived limits.

The study concludes with a short discussion of the influence of top decay observables on combined coupling limits, and the regions of the parameter space where single top cross sections still provide the crucial input to the bounds, namely the overall tbW vertex normalization and the interference direction $V_R \sim 2g_L$. In this respect, we address the impact of including V_L^{off} in the coupling basis, and briefly point out the possibilities to resolve the ambiguity between V_L and V_L^{off} experimentally, using kinematic distributions in the s channel.

ACKNOWLEDGMENTS

[1] F. Abe *et al.* (CDF Collaboration), Phys. Rev. Lett. **74**, 2626 (1995).

[2] S. Abachi *et al.* (D0 Collaboration), Phys. Rev. Lett. **74**, 2632 (1995).

[3] M. Lancaster (Tevatron Electroweak Working Group, for the CDF and D0 Collaborations), arXiv:1107.5255.

[4] V. Flyagin and V. Glagolev, Phys. Part. Nucl. **43**, 106 (2012).

[5] T. Aaltonen *et al.* (CDF Collaboration), Phys. Rev. Lett. **109**, 152003 (2012).

[6] T. Aaltonen *et al.* (CDF Collaboration, D0 Collaboration), Phys. Rev. D **85**, 71106 (2012).

[7] G. Aad *et al.* (ATLAS ollaboration), Eur. Phys. J. C **71**, 1577 (2011).

[8] S. Chatrchyan *et al.* (CMS Collaboration), Eur. Phys. J. C **71**, 1721 (2011).

[9] S. Chatrchyan *et al.* (CMS Collaboration), J. High Energy Phys. 07 (2011) 049.

[10] G. Aad *et al.* (ATLAS Collaboration), J. High Energy Phys. 05 (2012) 059.

[11] S. Chatrchyan *et al.* (CMS Collaboration), Phys. Rev. D **85**, 112007 (2012).

[12] G. Aad *et al.* (ATLAS Collaboration), Phys. Lett. B **717**, 89 (2012).

[13] S. Chatrchyan *et al.* (CMS Collaboration), arXiv:1209.3489.

[14] G. Aad *et al.* (ATLAS Collaboration), Tech. Report No. ATLAS-CONF-2011-104, Geneva, 2011.

[15] S. Chatrchyan *et al.* (CMS Collaboration), Phys. Rev. Lett. **107**, 091802 (2011).

[16] G. Aad *et al.* (ATLAS Collaboration), Phys. Lett. B **717**, 330 (2012).

[17] S. Chatrchyan *et al.* (CMS Collaboration), arXiv:1209.4533.

[18] F.-P. Schilling, Int. J. Mod. Phys. A **27**, 1230016 (2012).

[19] V. Chiochia, Mod. Phys. Lett. A **27**, 1230036 (2012).

[20] W. Buchmuller and D. Wyler, Nucl. Phys. **B268**, 621 (1986).

[21] C. Arzt, M. Einhorn, and J. Wudka, Nucl. Phys. **B433**, 41 (1995).

[22] G. Gounaris, M. Kuroda, and F. Renard, Phys. Rev. D **54**, 6861 (1996).

[23] G. Gounaris, D. Papadamou, and F. Renard, Z. Phys. C **76**, 333 (1997).

[24] L. Brzezinski, B. Grzadkowski, and Z. Hioki, Int. J. Mod. Phys. A **14**, 1261 (1999).

[25] K. Whisnant, J.-M. Yang, B.-L. Young, and X. Zhang, Phys. Rev. D **56**, 467 (1997).

[26] J.M. Yang and B.-L. Young, Phys. Rev. D **56**, 5907 (1997).

[27] B. Grzadkowski, Z. Hioki, K. Ohkuma, and J. Wudka, Nucl. Phys. **B689**, 108 (2004).

[28] J. Aguilar-Saavedra, Nucl. Phys. **B812**, 181 (2009).

[29] J. Aguilar-Saavedra, Nucl. Phys. **B821**, 215 (2009).

[30] J. Aguilar-Saavedra, Nucl. Phys. **B843**, 638 (2011).

[31] B. Grzadkowski, M. Iskrzynski, M. Misiak, and J. Rosiek, J. High Energy Phys. 10 (2010) 085.

[32] C. Arzt, Phys. Lett. B **342**, 189 (1995).

[33] S. Weinberg, Phys. Lett. **91B**, 51 (1980).

[34] J. Gasser and H. Leutwyler, Ann. Phys. (N.Y.) **158**, 142 (1984).

[35] H. Georgi, Nucl. Phys. **B361**, 339 (1991).

[36] A. De Rujula, M. Gavela, P. Hernandez, and E. Masso, Nucl. Phys. **B384**, 3 (1992).

[37] J. Aguilar-Saavedra, Nucl. Phys. **B804**, 160 (2008).

[38] W. Kilian, T. Ohl, and J. Reuter, Eur. Phys. J. C **71**, 1742 (2011).

[39] F. del Aguila and J. Aguilar-Saavedra, Phys. Rev. D **67**, 014009 (2003).

[40] J. Aguilar-Saavedra, J. Carvalho, N. F. Castro, F. Veloso, and A. Onofre, Eur. Phys. J. C **50**, 519 (2007).

[41] J. Aguilar-Saavedra, J. Carvalho, N. F. Castro, A. Onofre, and F. Veloso, Eur. Phys. J. C **53**, 689 (2008).

[42] K.-m. Cheung, Phys. Rev. D **53**, 3604 (1996).

[43] Z. Hioki and K. Ohkuma, Eur. Phys. J. C **65**, 127 (2010).

[44] D. Choudhury and P. Saha, Pramana **77**, 1079 (2011).

[45] D.-W. Jung, P. Ko, J. S. Lee, and S.-h. Nam, Phys. Lett. B **691**, 238 (2010).

[46] E. Gabrielli and M. Raidal, Phys. Rev. D **84**, 054017 (2011).

[47] C. Burges and H.J. Schnitzer, Nucl. Phys. **B228**, 464 (1983).

[48] C.N. Leung, S. Love, and S. Rao, Z. Phys. C **31**, 433 (1986).

[49] B. Grzadkowski, Z. Hioki, and M. Szafranski, Phys. Rev. D **58**, 035002 (1998).

[50] Q.-H. Cao, J. Wudka, and C.-P. Yuan, Phys. Lett. B **658**, 50 (2007).

[51] E. L. Berger, Q.-H. Cao, and I. Low, Phys. Rev. D **80**, 074020 (2009).

[52] J. Aguilar-Saavedra, M. Fiolhais, and A. Onofre, J. High Energy Phys. 07 (2012) 180.

[53] B. Grzadkowski and M. Misiak, Phys. Rev. D **78**, 077501 (2008).

[54] J. Drobnak, S. Fajfer, and J. F. Kamenik, Nucl. Phys. **B855**, 82 (2012).

[55] J. Drobnak, S. Fajfer, and J. F. Kamenik, Phys. Lett. B **701**, 234 (2011).

[56] C. Zhang, N. Greiner, and S. Willenbrock, Phys. Rev. D **86**, 014024 (2012).

[57] J. Pumplin, D.R. Stump, J. Huston, H.-L. Lai, P. Nadolsky, and W.-K. Tung, J. High Energy Phys. 07 (2002) 012.

[58] V. M. Abazov *et al.* (D0 Collaboration), Phys. Rev. D **85**, 091104 (2012).

[59] N. Kidonakis, Phys. Rev. D **81**, 054028 (2010).

[60] N. Kidonakis, Phys. Rev. D **83**, 091503 (2011).

[61] Z. Sullivan, Phys. Rev. D **70**, 114012 (2004).

[62] E. Boos, V. Bunichev, L. Dudko, V. Savrin, and A. Sherstnev, Phys. At. Nucl. **69**, 1317 (2006).

[63] P. Falgari, F. Giannuzzi, P. Mellor, and A. Signer, Phys. Rev. D **83**, 094013 (2011).

[64] J. M. Campbell and R. K. Ellis, arXiv:1204.1513.

[65] J. Gao, C. S. Li, L. L. Yang, and H. Zhang, Phys. Rev. Lett. **107**, 092002 (2011).

[66] J. Drobnak, S. Fajfer, and J. F. Kamenik, Phys. Rev. D **82**, 114008 (2010).

[67] G. Aad *et al.* (ATLAS Collaboration), J. High Energy Phys. 06 (2012) 088.

[68] E. Boos, V. Bunichev, L. Dudko, and M. Perfilov, Phys. Lett. B **655**, 245 (2007).

[69] G. Aad *et al.* (ATLAS Collaboration), Tech. Report No ATLAS-CONF-2011-118, Geneva, 2011.